INSTITUTO NACIONAL DE CÂNCER JOSÉ ALENCAR GOMES DA SILVA

PROGRAMAS DE RESIDÊNCIA MULTIPROFISSIONAL EM ONCOLOGIA E RESIDÊNCIA EM FÍSICA MÉDICA

ALAINE FERREIRA GRIGIO RAMOS

DEVELOPMENT OF DIGITAL ANTHROPOMORPHIC BREAST SIMULATORS FOR 3D PRINTING

RIO DE JANEIRO, RJ

2023

ALAINE FERREIRA GRIGIO RAMOS

Development of Digital Anthropomorphic Breast Simulators for 3D Printing

Trabalho de Conclusão de Curso apresentado ao Instituto Nacional de Câncer José Alencar Gomes da Silva do Ministério da Saúde (Brasil), para a obtenção do grau de especialista em Física Médica com ênfase em Imagem.

Orientador: Dr. Rafael Pohlmann Figueiredo Simões

RIO DE JANEIRO

2023

Abstract

Objective: To provide STL files for 3D printing of enhanced anthropomorphic breast simulators, including various tumour sizes, to improve mammography quality and breast cancer diagnosis accuracy.

Methods: This study involved a bibliographical review encompassing breast classifications, focusing on the most common and challenging in mammography. Breast tissue density data was collected to select similar 3D printing materials. Manipulation of breast models from a repository was carried out in the 3D Builder software with defined skin and adipose tissue thicknesses. Tumors were sized in eleven different dimensions.

Results: The importance of selecting dense and high glandular density breasts, which represent a significant portion of the population at high risk of breast cancer, was highlighted. Literature data on breast tissue densities and the choice of suitable 3D printing materials were crucial in creating realistic breast simulators, resulting in models of dense and fatty breasts as well as tumours of different sizes. The final files are available on the OneDrive platform for public access, providing a simulator with densities similar to real ones, contributing to the assessment of mammography image quality and enabling future tests with artificial intelligence in the detection of minimal tumours.

Conclusion: The availability of anthropomorphic breast models in STL format for 3D printing offers a valuable tool in the field of radiology, enabling more objective assessments of image quality in mammography. These simulators allow for more rigorous testing, potentially enhancing diagnostic accuracy. Furthermore, in the future, they can be used to assess the limits of microcalcification detection by artificial intelligence, contributing to advancements in breast cancer detection.

Keywords: 3D Printing, Breast Phantoms, Image Quality, Breast Cancer Detection.

Introduction

Cancer is a condition characterized by uncontrolled cellular growth in various areas of the body, which can result from genetic predisposition related to cancer or cumulative damage to genetic material caused by physical, chemical, or biological factors [1]. The incidence of this disease has become increasingly common, with projections indicating approximately 704,000 new cancer cases in Brazil from 2023 to 2025, with breast cancer representing a significant portion, accounting for around 73,000 new cases. This presents a considerable challenge to public health, especially due to limited access to early diagnosis technologies for this type of cancer, which could impact survival rates [2], [3].

Among the various technologies available for breast cancer detection through medical imaging, mammography stands out as a crucial examination for the early identification of this disease. Mammography is an imaging procedure that uses X-rays to capture images of the patient's breast and axilla to identify potential abnormalities, such as nodules or microcalcifications, which may indicate the presence of breast cancer [4]. This examination is often uncomfortable and, in some cases, painful due to the need to compress the breast to ensure uniform penetration of radiation into breast tissue, resulting in more homogeneous images. This compression also minimizes patient movement to avoid blurriness in the image, enhances image sharpness, reduces tissue overlap, and provides a clearer image of the breast, identifying nodules or other abnormalities even before they are palpable during a physical examination [5]–[7]. Nonetheless, mammography is not infallible and can lead to false positives, where an abnormal examination is identified, but there is no cancer, or false negatives, where a normal examination is identified, but cancer is present [8]. According to studies, the rate of false negatives in mammography examinations can reach up to 35% [9]. However, despite these limitations, mammography remains the most critical examination in population screening for early breast cancer detection.

Due to the diagnostic significance of this procedure, mammography machines are subject to quality control programs, which encompass regular tests to ensure proper functioning and produce accurate and reliable images [10]. These tests include tube and image quality tests, as well as other essential evaluations such as radiation dose assessments and overall equipment performance tests. Tube quality tests are conducted to ensure that the X-ray tube is producing X-rays within the correct energy range and that the tube is functioning correctly. Image quality tests, on the other hand, are performed to ensure that the images generated by the mammography machine are sharp, clear, and accurate [11]. These image quality tests use a simulator object (phantom) to assess image quality in terms of spatial resolution, contrast, and noise [12], [13]. Thus, they are important tests to ensure that the mammography machine is producing images of sufficient quality to aid in breast cancer diagnosis [14].

There are different types of simulators used in the quality control of mammography devices, with notable examples employed by the Brazilian College of Radiology - CBR,

the American College of Radiology - ACR, and the Mammo FFDM phantom from CIRS. The CBR simulator reproduces a compressed breast with a thickness of 40 to 50 mm, internally presenting microcalcifications, fibres, low-contrast disks, and tumour masses. In turn, the ACR phantom simulates a compressed breast of 42 mm, containing nylon fibres, microcalcifications, and tumour masses. Finally, the Mammo FFDM Phantom Simulator from CIRS is a simulator with a thickness of 42 mm, composed of microcalcifications, fibres, and tumour masses varying in dimensions from 0.20 to 1 mm.

In addition to these simulators, there is the Patricia Mora simulator in collaboration with the IAEA – International Atomic Energy Agency, with a thickness of 50 mm, composed of Cu and Al plates. The NORMI MAM digital simulator from PTW, with a thickness of 40 mm, is composed of an Al plate, and the CDMAM 3.4 simulator from Capintec, with a thickness of 40 mm, is composed of gold disks arranged in a matrix. These simulators assess contrast and resolution, thus testing the imaging system's ability to detect density differences between normal breast tissue and suspicious lesions, such as tumours. Additionally, they evaluate the imaging system's ability to distinguish between small details in an image, which can affect the ability to detect early-stage breast lesions[15]–[17].

Thus, this work aims to contribute to the field of radiology by providing easy access to anthropomorphic breast simulator models for 3D printing, including different physical formats, compressed, and natural. This is particularly relevant due to the unavailability of 3D printing materials with sufficient flexibility to be compressed in the mammography equipment. It also includes suggestions for printing materials with the aim of subsequent validation.

Material and Methods

A bibliographical review was conducted, addressing the various classifications of breast types, with a focus on the type with the highest incidence of cancer and those that present the greatest challenge in visualizing tumours in mammograms due to their specific characteristics. Additionally, an investigation into the density of breast tissues, such as adipose tissue, glandular tissue, tumour tissue, and skin, was carried out to use this data for the selection of 3D printing materials and fill materials that closely approximate the natural densities of a standard breast, thereby providing greater fidelity to the anthropomorphic breast simulator.

Following the results of these bibliographical studies, the "Repository of Anthropomorphic Numerical Breast Models" [18] where the authors constructed models based on acquisitions from 3 Tesla Magnetic Resonance Imaging, employing a 3D modelling methodology comprising three phases: 3D breast mask generation, 3D segmentation based on clustering, and mapping of these clusters to the dielectric properties of breast tissues. This process resulted in models that provide information about the spatial distribution of tissues in the breast, enabling the breast's shape and complexity to be reconfigurable. The models available in this repository come in various formats such as raw data, mat, and STL. However, we exclusively utilized the folder

containing solid models, which includes STL files featuring diverse mammary complexities, including the presence of a tumour. Among the array of available mammary complexities, we selected the two most relevant and common types, as indicated by literature, for subsequent manipulation.

For the manipulation of these selected files, Microsoft's 3D Builder software was employed. During the manipulation process, dimensions such as skin and adipose tissue thickness, as per the literature, were defined to create a shell with skin thickness and a second STL file with adipose tissue thickness, allowing for proper fitting after printing. Furthermore, the tumour file was resized into eleven different sizes, namely 0.75, 0.60, 0.50, 0.45, 0.40, 0.35, 0.30, 0.25, 0.20, 0.15, and 0.10 mm. The initial size of 0.75 mm was chosen following Regulatory Instruction No. 92 [19], which regulates mammography equipment in Brazil for the evaluation of image quality. For both selected breast types, two distinct forms were created: one representing the compressed breast, a necessary positioning for the proper application of mammographic technique, and another simulating the breast in its natural shape.

With the prepared STL files, the next step involved researching commercially available 3D printing materials that had densities close to those of the tissues that would be printed in the future. This included the search for materials that could be used in resin form, with a density similar to fibroglandular tissue, to fill the phantom after printing, to obtain a simulator that encompasses all the tissues that constitute a diseased breast in their respective tissue-equivalent materials, including tumours of different sizes.

Results

According to the reference, dense breasts, characterized by high glandular density, affect approximately 43% of the general population [20]. This type of breast presents the greatest complexity in distinguishing between healthy tissue and potentially diseased areas during mammographic examinations. Furthermore, this breast type carries a high risk of cancer [21]. On the other hand, according to another reference, fatty breasts, characterized by low glandular density, are the most common and are associated with various factors, including high Body Mass Index (BMI) values [22]. Therefore, the choice to provide STL files for 3D printing focused on these two breast types.

In the literature review, we found density values for each of the tissues that make up the breast, which are detailed in Table 1. As mentioned in the literature, skin density is considered equivalent to the density of fibroglandular tissue, justified by the density measurement procedures for the skin, which involve freezing and thawing of samples, which can compromise measurement reliability [23]. Therefore, for reasons of safety and accuracy, the same density as fibroglandular tissue was chosen to represent the skin. Table 1 also presents a variety of commercially available materials for 3D printing, along with their respective densities, which are close to the densities of breast tissues. This work recommends printing a test specimen to measure the density of these materials post-printing. In the case of fibroglandular tissue, an appropriate liquid resin option was sought

to fill the simulator after printing, as the file provided by the repository was excessively complex, making its printing unfeasible.

Tissues	D(tis) [g/cm³]	Material	D(mat) [g/cm³]
Adipose	0,932[23]	Sensitive Resin	0,8 a 0,9[24]
	0,928[25]	TangoPlus	1,12 a 1,13[26], [27]
Fibroglandular	1,066[23]	Resina 4230 Epoxi	1,05[28]
Tumour	1,044[25]	HIPS	1,03[29]
	1,044[23]	ABS	1,04[30]
Skin	Fibroglandular[23]	ASA	1,05[31]
	1,066[23]	-	-

Table 1: Densities of breast tissues and commercially available 3D printing materials found in the literature.

As highlighted by Alexander & Miller [32], the thickness of the skin varies from 0.82 mm to 1.19 mm. Therefore, we chose to use the average of these values, which corresponds to approximately 1 mm in thickness to represent the skin. As for the amount of fat, a study conducted by Diniz ALD et al. [33], revealed a subcutaneous fat thickness of approximately 26.4 mm. This measurement was adopted for the breast phantom with higher fat content, while for the dense breast phantom, half of this value was selected, equivalent to 13.2 mm of adipose tissue thickness.

With the skin and fat thicknesses defined, the STL files provided by the repository were manipulated as explained in the methodology, resulting in what can be seen in Figures 1, 2, and 3, which depict the dense breast at thicknesses of 45 mm and 100 mm, the fatty breast at a thickness of 45 mm and 100 mm, and a tumour, respectively.
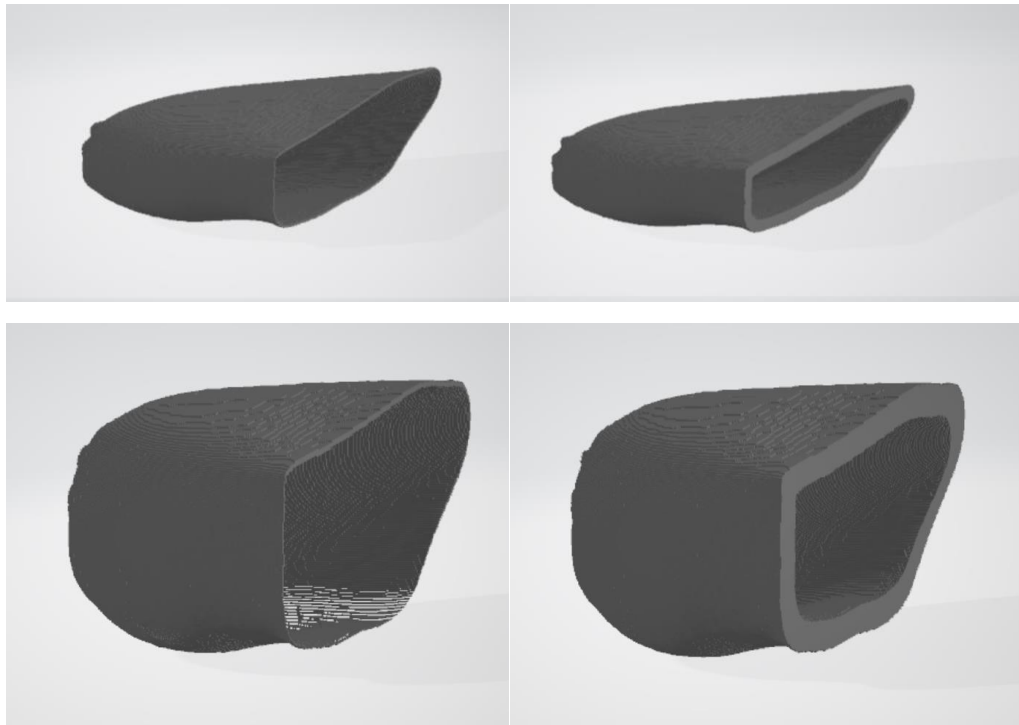
Figure 1: STL files of breast skin and fat with high glandular density, manipulated with thicknesses of 45 mm and 100 mm.
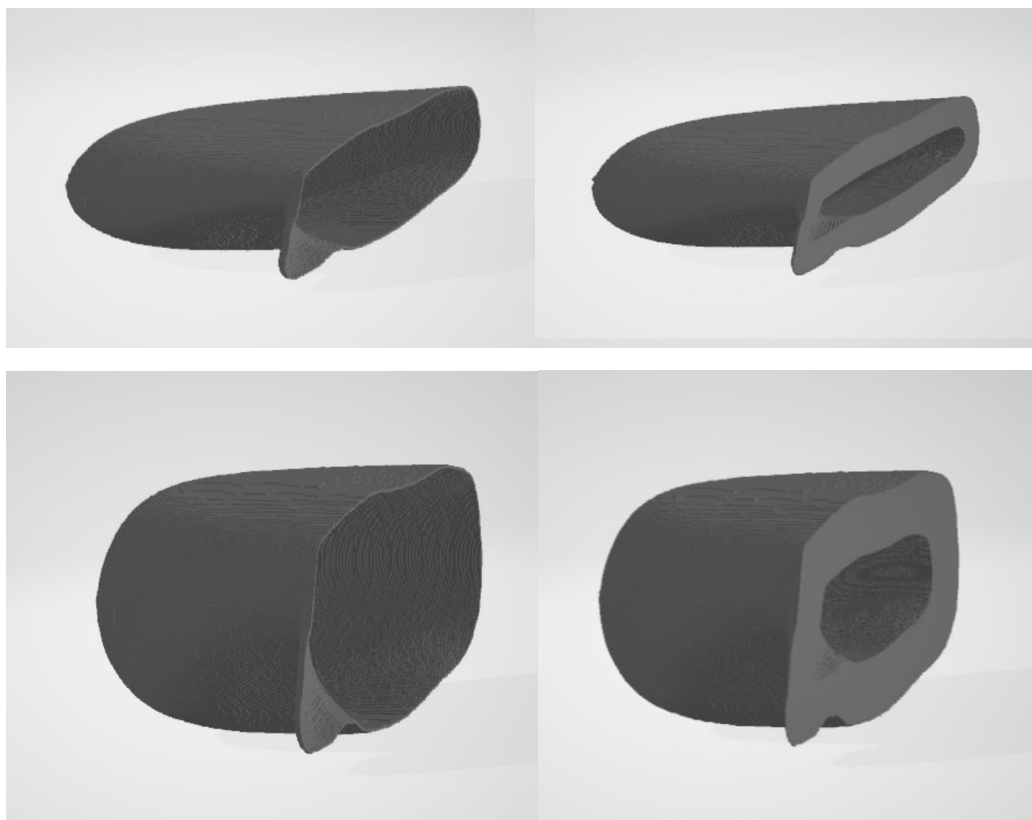

Figure 2: STL files of breast skin and fat with low glandular density, manipulated with thicknesses of 45 mm and 100 mm.
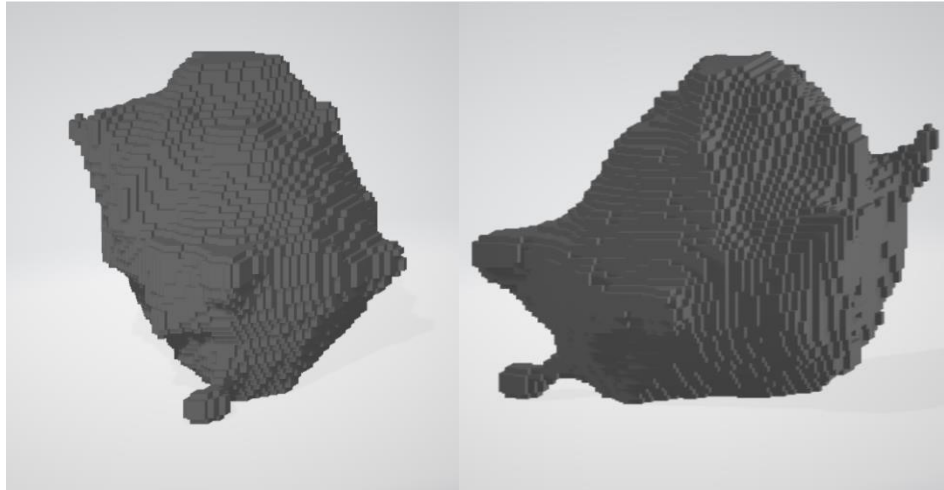
Figure 3: STL file of the breast tumour.

The location and further explanation of the dataset are described in the supplementary materials section.

Discussion

Given the importance of using simulators in evaluating the image quality of mammography, it would be beneficial to create a device with equivalent tissue material to achieve a more realistic simulation. Additionally, a 3D-printed anthropomorphic phantom would allow for control over the position and dimension of its tumour masses, which traditional commercial simulators do not permit. Tumour masses in traditional simulators are always in the same location, sometimes causing biased assessments. With control over the tumour mass dimensions, we can also identify the equipment's spatial resolution limit and use images obtained by this anthropomorphic simulator as training material for AI algorithms.

Based on the results from the literature, which point to the prevalence of breasts with high glandular density, posing a challenge in distinguishing healthy tissue from diseased tissue, and the higher incidence of breasts with low glandular density and more adipose tissue, we chose to focus on manipulating files that met these criteria among other options available in the central repository of this study.

During the process of manipulating these files for 3D printing, it was noted that the STL file containing information about fibroglandular tissue had a complexity that made precise printing difficult. In this regard, we sought alternatives in the literature and identified the 4230 Epoxy resin, with a density of 1.05 g/cm³, which closely approximates the density of real fibroglandular tissue, which is 1.066 g/cm³. To overcome this challenge, we geometrically adapted the STL files representing the skin and adipose tissue so that they could be properly fitted after printing, and the 4239 Epoxy resin will be used to fill the phantom representing fibroglandular tissue. In the case of the STL files representing tumours, each was scaled according to its real scale and varied dimensions, allowing for post-print insertion into the phantom.

During the development of these files, we also considered practical limitations related to tumour dimensions. The issue of the availability of printers with the necessary resolution to print a tumour of 0.10 mm deserves attention. If this resolution is not available, we suggest printing the tumour to the maximum dimension possible with the printer. It is relevant to note that, following national regulatory standards, the minimum size of a tumour that should be visualized is established at 0.75 mm, which is the initial size of the tumours to be inserted into the phantom developed in this work. Additionally, for informational purposes, the IAEA document - TECDOC-1958 states that the minimum visibility limit of structures should be per the one established by the phantom manufacturer. In contrast, the European Guide for Quality Control in Mammography requests a comparison of structure visibility with the baseline obtained during equipment acceptance evaluation. Finally, the American College of Radiology indicates that the minimum visibility limit for masses is 0.60 mm [34]-[36]. Printing tumours at minimum dimensions is justified by the potential future use of the images acquired by this phantom to test the ability of artificial intelligence algorithms to detect tumours that may not be perceptible to the human eye.

By considering the information obtained in the literature regarding breast tissue densities and the availability of commercial materials, we have successfully produced a phantom with densities closer to real conditions. This approach fills an important gap, as the reference phantoms developed by the ACR for mammography do not include this characteristic. With our realistic and anthropomorphic simulator, it becomes feasible to assess the accuracy of equipment under conditions closer to those encountered in clinical practice.

This approach represents a significant advancement in improving the accuracy and quality of mammography exams. It fosters the development of more effective technologies for the early diagnosis of breast cancer, enabling an in-depth analysis of human visualization capabilities, particularly concerning extremely small microcalcifications. Furthermore, the possibility of testing the capabilities of artificial intelligence algorithms in the recognition of minimal tumours opens up new prospects in the quest for even more precise and efficient diagnoses, thereby reducing the rate of false negatives in mammography exams.

Conclusion

In this work, we provided a realistic anthropomorphic breast model based on tumour incidence and breast type classifications, that can be 3D-printed and used for further characterization of mammography devices and data production for artificial intelligence model development and testing.

Statements

References

[1]   H.-O. Adami, N. E. Day, D. Trichopoulos, and W. C. Willett, "Primary and secondary prevention in the reduction of cancer morbidity and mortality," Eur J Cancer, vol. 37, pp. 118–127, Sep. 2001, doi: 10.1016/S0959-8049(01)00262-3.

[2]   M. de O. Santos, F. C. da S. de Lima, L. F. L. Martins, J. F. P. Oliveira, L. M. de Almeida, and M. de C. Cancela, "Estimativa de Incidência de Câncer no Brasil, 2023-2025," Revista Brasileira de Cancerologia, vol. 69, no. 1, Feb. 2023, doi: 10.32635/2176-9745.RBC.2023v69n1.3700.

[3]   Y. C. Barbosa, A. G. C. Oliveira, P. P. C. Rabêlo, F. de S. Silva, and A. M. dos Santos, "Fatores associados à não realização de mamografia: Pesquisa Nacional de Saúde, 2013," Revista Brasileira de Epidemiologia, vol. 22, 2019, doi: 10.1590/1980-549720190069.

[4]   A. S. Majid, E. S. de Paredes, R. D. Doherty, N. R. Sharma, and X. Salvador, "Missed Breast Carcinoma: Pitfalls and Pearls," RadioGraphics, vol. 23, no. 4, pp. 881–895, Jul. 2003, doi: 10.1148/rg.234025083.

[5]   R. van Engen, S. van Woudenberg, H. Bosmans, K. Young, and M. Thijssen, The European protocol for the quality control of the physical and technical aspects of mammography screening: part B - Digital mammography, 4o., vol. 1.22. European Guidelines for Breast Cancer Screening, 2006.

[6]   IAEA, Quality Assurance Programme Digital Mammography, vol. 17. IAEA - AGÊNCIA INTERNACIONAL DE ENERGIA ATÔMICA, Human Health Series, 2011.

[7]   N. MOSHINA, S. SEBUODEGARD, and S. HOFVIND, "Is breast compression associated with breast cancer detection and other early performance measures in a population-based breast cancer screening program," Breast Cancer Res Treat, vol. 163, pp. 605–613, 2017.

[8]   INCA, Assistência de alta complexidade em oncologia: diretrizes para o controle de câncer na rede de atenção à saúde. Rio de Janeiro, 2017.

[9]   J. A. Harvey, L. L. Fajardo, and C. A. Innis, "Previous mammograms in patients with impalpable breast carcinoma: retrospective vs blinded interpretation. 1993 ARRS President's Award.," American Journal of Roentgenology, vol. 161, no. 6, pp. 1167–1172, Dec. 1993, doi: 10.2214/ajr.161.6.8249720.

[10]   M. J. Yaffe, "Developing a quality control program for digital mammography: achievements so far and challenges to come," Imaging Med, vol. 3, no. 1, pp. 123–133, Feb. 2011, doi: 10.2217/iim.10.63.

[11]   N. Richli Meystre et al., "Characterization of radiographers' mammography practice in five European countries: a pilot study," Insights Imaging, vol. 10, no. 1, p. 31, Dec. 2019, doi: 10.1186/s13244-019-0711-0.

[12]   M. A. Pinheiro, C. D. de Almeida, J. E. Peixoto, M. D. A. S. Valverde, and A. V. Marin, "Análise das tecnologias e doses glandulares médias em mamografia no Brasil no período de 2011 a 2016," Brazilian Journal of Radiation Sciences, vol. 6, no. 3, Sep. 2018, doi: 10.15392/bjrs.v6i3.653.

[13]   L. C. H. Campos, "Avaliações de qualidade aplicadas na comparação de sistemas mamográficos digitais e convencionais," Universidade de São Paulo, São Carlos, 2008. doi: 10.11606/D.18.2008.tde-04072008-094950.

[14]   R. Jayadevan, M. J. Armada, R. Shaheen, C. Mulcahy, and P. J. Slanetz, "Optimizing Digital Mammographic Image Quality for Full-Field Digital Detectors: Artifacts Encountered during the QC Process," RadioGraphics, vol. 35, no. 7, pp. 2080–2089, Nov. 2015, doi: 10.1148/rg.2015150036.

[15]   L. A. B. AMARAL, "Desenvolvimento de um simulador mamográfico flexível com microcalcificações simuladas.," 2010.

[16]   "Fantoma Mamográfico de Acreditação ACR Phantom." Accessed: Dec. 15, 2023. [Online]. Available: https://www.marcamedica.com.br/fantoma-mamografico-de-acreditacao-acr-phantom/

[17]   " Nuclear Medicine Product Catalog - Capintec - Catálogo | Documentação técnica | Folheto." Accessed: Dec. 15, 2023. [Online]. Available: https://pdf.medicalexpo.com/pt/pdf-en/capintec/2015-nuclear-medicine-product-catalog/70709-150760.html#open559909

[18]   M. Omer and E. Fear, "Anthropomorphic breast model repository for research and development of microwave breast imaging technologies," Sci Data, vol. 5, 2018, doi: 10.1038/sdata.2018.257.

[19]   Ministério da Saúde, Agência Nacional de Vigilância Sanitária, and Diretoria Colegiada, "INSTRUÇÃO NORMATIVA - IN No 92, DE 27 DE MAIO DE 2021." pp. 153–153, 2021.

[20]   C. I. Lee, L. W. Bassett, and C. D. Lehman, "Breast Density Legislation and Opportunities for Patient-centered Outcomes Research," Radiology, vol. 264, no. 3, pp. 632–636, Sep. 2012, doi: 10.1148/radiol.12120184.

[21]   N. F. Boyd et al., "Mammographic Density and the Risk and Detection of Breast Cancer," New England Journal of Medicine, vol. 356, no. 3, pp. 227–236, Jan. 2007, doi: 10.1056/NEJMoa062790.

[22]   K. Kerlikowske et al., "Outcomes of Screening Mammography by Frequency, Breast Density, and Postmenopausal Hormone Therapy," JAMA Intern Med, vol. 173, no. 9, p. 807, May 2013, doi: 10.1001/jamainternmed.2013.307.

[23]   J. Said Camilleri et al., "Review of Thermal and Physiological Properties of Human Breast Tissue," Sensors, vol. 22, no. 10, p. 3894, May 2022, doi: 10.3390/s22103894.

[24]   China, "SAFETY DATA SHEET FOR CHEMICAL PRODUCTS," 2017. Accessed: Oct. 09, 2023. [Online]. Available: www.nbtscn.com

[25]   P. C. Johns and M. J. Yaffe, "X-ray characterisation of normal and neoplastic breast tissues," Phys Med Biol, vol. 32, no. 6, pp. 675–695, Jun. 1987, doi: 10.1088/0031-9155/32/6/002.

[26]   N. Kiarashi et al., "Development of realistic physical breast phantoms matched to virtual breast phantoms based on human subject data," Med Phys, vol. 42, no. 7, pp. 4116–4126, Jul. 2015, doi: 10.1118/1.4919771.

[27]   "PolyJetTM Materials Reference Guide." Accessed: Sep. 26, 2023. [Online]. Available: https://static1.squarespace.com/static/5f7b28de8cf6fe0f89e02bdf/t/5f7dad2c094eac3ec0b10ae1/1602071886713/PolyJet+Materials+Reference+Guide.pdf

[28]   "Resina 4230 Epoxi Transparente Para Altas Espessuras Com Proteção UV Com Endurecedor (1,180 Kg) - Redelease", Accessed: Sep. 26, 2023. [Online]. Available: https://www.redelease.com.br/resina-epoxi-transparente-para-altas-espessuras-com-protec-o-uv-1-180-kg.html.html

[29]   "datasheet_hips_extrafill", Accessed: Sep. 27, 2023. [Online]. Available: https://www.materialpro3d.cz/user/documents/upload/datasheet_hips_extrafill.pdf

[30]   "TDS_BCN3D_Filaments_ABS." Accessed: Sep. 26, 2023. [Online]. Available: https://3dprint.pe/wp-content/uploads/2018/09/TDS_BCN3D_Filaments_ABS.pdf

[31]   "ASA Filament." Accessed: Sep. 27, 2023. [Online]. Available: https://static.treatstock.com/static/fxd/wikiMaterials/ASA/files/tds_asa_filament.pdf

[32]   H. Alexander and D. L. Miller, "Determining Skin Thickness with Pulsed Ultra Sound," Journal of Investigative Dermatology, vol. 72, no. 1, pp. 17–19, Jan. 1979, doi: 10.1111/1523-1747.ep12530104.

[33]   Diniz ALD, Tomé RAF, Debs CL, Carraro R, Roever LB, and Pinto RMC, "Reproducibility of ultrasonography as a method to measure abdominal and visceral fat," Radiol Bras, vol. 42, no. 6, pp. 353–357, 2009.

[34]   IAEA-TECDOC-1058. Protocolos de control de calidad para radiodiagnóstico en américa latina y el caribe. International Atomic Energy Agency.

[35]   Guia Europeu. European protocol for the quality control of the physical and technical aspects of mammography screening. European guidelines for quality assurance in breast cancer screening and diagnosis. Fourth edition.

[36]   AMERICAN COLLEGE OF RADIOLOGY. Mammography quality control manual. ACR – Committee on Quality Assurance in Mammography, 1999.

Supplementary Materials

The dataset has been stored in the Zonedo platform under the DOI (**10.5281/zenodo.10852818**). In this platform was possible to provide the manipulated stl files for free and openly to the public. On this platform, uploaded a zip file with folders named 'Breast_Phantom,' which is subdivided into three subfolders: 'High_density_breast,' 'Low_density_breast,' and 'Tumors,' as shown in Figure 4. Within the "High_density_breast ' subfolder, there are two additional subfolders: "High_density_breast_45' and "High_density_breast_100.' These subfolders represent, respectively, the breast in the compressed format (for mammography simulation) with a total thickness of 45 mm and in the natural format with a thickness of 100 mm. In each of these subfolders, there are two stl files: 'Fat_high_density_45' and 'Skin_high_density_45' or 'Fat_high_density_100' and 'Skin_high_density_100.' These files represent, respectively, adipose tissue and skin. Within the 'Low_density_breast' subfolder, as demonstrated in Figure 5, we have adopted a similar organization to the 'High_density_breast' subfolder. However, the files in this subfolder represent a breast with low glandular density. In the 'Tumors' subfolder, all stl files are available in various dimensions ranging from 0.75 to 0.10 mm in their largest dimension, as illustrated in Figure 6.

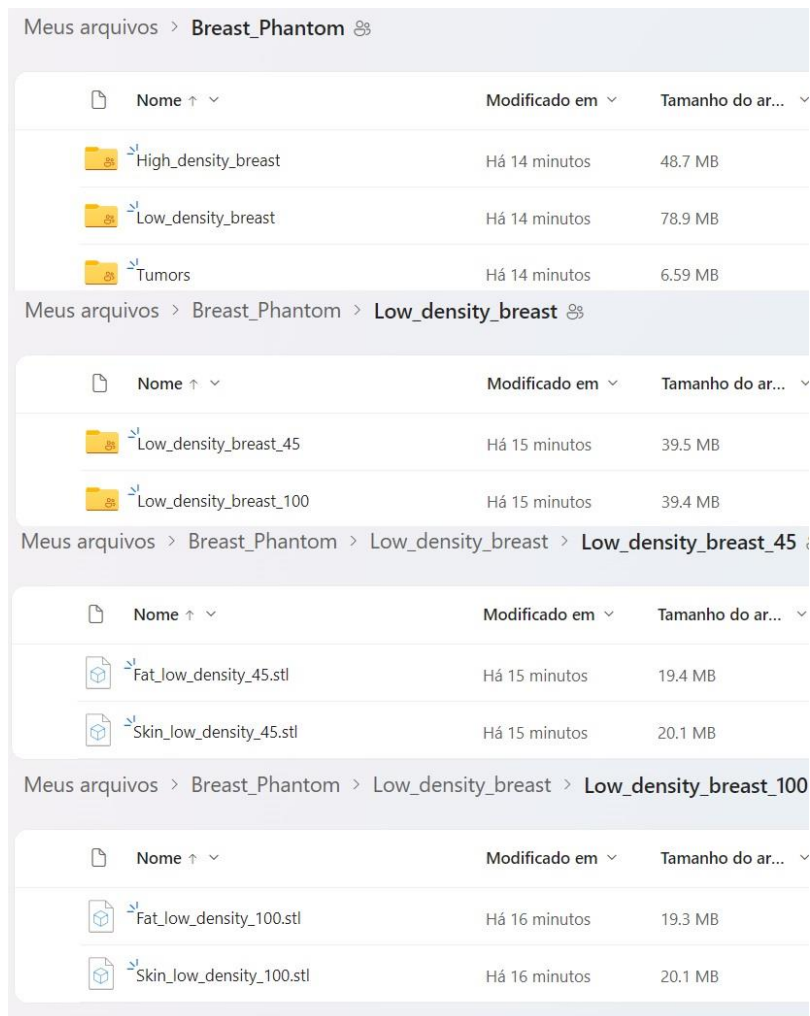Figure 4: Folders arrangement for high glandular density breast on the platform.

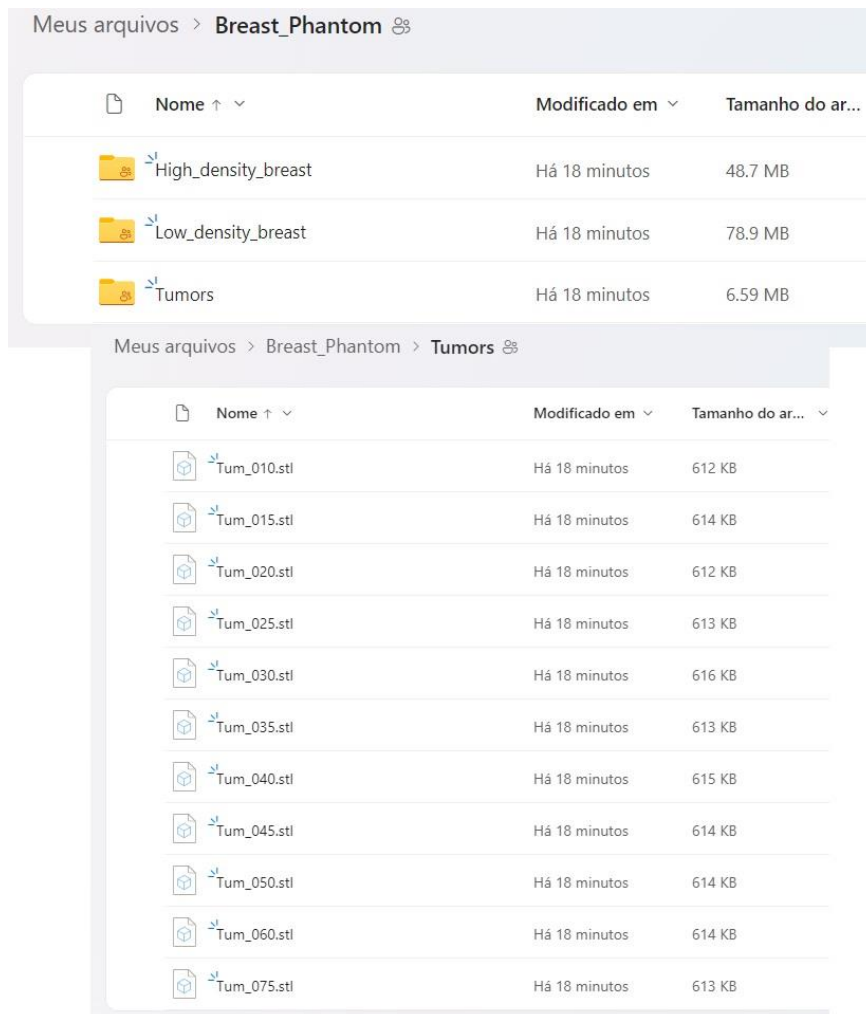Figure 5: Folders arrangement for low glandular density breast on the platform.

Figure 6: Folders arrangement for tumors of different dimensions on the platform.